New Journal of Physics
The open-access journal for physics

Determination of the photoelectron reference plane in nanostructured surfaces

Jorge Lobo-Checa[1,7], Aitor Mugarza[2], José Enrique Ortega[3,4,5] and Enrique G Michel[6]

[1] Centre d'Investigació en Nanociència i Nanotecnologia, CIN2 (CSIC-ICN), Esfera UAB, Campus de la UAB, 08193-Bellaterra, Spain
[2] Catalan Institute of Nanotechnology (ICN-CIN2), Campus de la UAB, E-08193 Bellaterra, Spain
[3] Dpto Física Aplicada I, Universidad del País Vasco, E-20018 San Sebastián, Spain
[4] Centro de Física de Materiales CSIC/UPV-EHU-Materials Physics Center, Manuel Lardizabal 5, E-20018 San Sebastián, Spain
[5] Donostia International Physics Center, Paseo Manuel Lardizabal 4, E-20018 Donostia-San Sebastián, Spain
[6] Dpto de Física de la Materia Condensada and Instituto Universitario de Ciencia de Materiales 'Nicolás Cabrera', Universidad Autónoma de Madrid, 28049 Madrid, Spain
E-mail: jorge.lobo@cin2.es

New Journal of Physics **13** (2011) 103013 (14pp)
Received 3 June 2011
Published 12 October 2011
Online at http://www.njp.org/
doi:10.1088/1367-2630/13/10/103013

Abstract. In angle-resolved photoemission (ARPES) from crystalline solids, wave-vector conservation applies to the two-dimensional (2D) surface, which may thus be defined as the reference plane in ARPES. We investigate whether such reference varies for photoemitted electrons in nanometer-sized systems that expose different crystal planes. To this aim, we exploit the structural tunability of the Ag/Cu(223) system which is capable of offering surfaces with periodic arrays of nanofacets of varying size and orientation. A thorough, photon-energy-dependent analysis of the surface states confined to such nanostructures is performed comparing different reference planes for photoemitted electrons. Assuming the premise that $k_{||}$ must be a good quantum number for 2D states, we conclude that the (final state) photoelectron reference direction is not the average optical direction but the local facet that confines the (initial state) surface

[7] Author to whom any correspondence should be addressed.

electrons. Moreover, in the general case of nanostructured systems with uneven surfaces, we show how the photoelectron reference plane can be empirically determined through such a photon-energy-dependent ARPES analysis.

Contents

1. Introduction

Surfaces offer an excellent platform for the self-assembly of solid nanostructures, such as nanodots, atomic wires or nanostripes [1–7]. In general, self-organization results in textured surfaces that expose different crystal planes. Examples are nanostripe arrays, which can be created by step decoration [8, 9] and faceting of stepped surfaces [10–13]. On the other hand, for reasonable size distributions of nano-object arrays characterized by their electron confinement, angle-resolved photoemission (ARPES) appears to be a well-suited technique for addressing the electronic structure of individual nano-units. However, non-planar geometries, such as that of textured, nanostructured arrays, pose an interesting question: can momentum conservation rules be applied in a straightforward way, as for a flat solid surface, or must the local geometry be taken into consideration in order to analyze the photoemission signal from the individual nano-objects?

In ARPES, energy and momentum conservation is applied to photoemitted electrons at the solid/vacuum interface [14]. Assuming free-electron-like final states, the following expressions for the parallel and perpendicular components of the electron momentum inside the crystal are obtained:

$$k_{||} = \sqrt{\frac{2m_e}{\hbar^2} E_{kin} \sin^2\theta}, \tag{1}$$

$$k_{\perp} = \sqrt{\frac{2m_e}{\hbar^2} (E_{kin} \cos^2\theta + V_0)}, \tag{2}$$

where m_e is the electron mass and V_0 is the crystal inner potential [15–17]. E_{kin} and θ are the two relevant magnitudes measured in ARPES. They are, respectively, the kinetic energy of the

photoelectron and the electron emission angle from the solid. The two wave vector components $k_{||}$ and $k_{\perp}$, and hence the photoelectron emission angle θ, are defined with respect to the crystal plane at which $k_{||}$ is strictly conserved, namely the solid/vacuum interface plane. Although such a reference plane is well defined on atomically flat surfaces, it is not clear whether equations (1) and (2) apply to the case of surfaces corrugated at the scale of the coherence length of the photoemission process. In other words, we should experimentally determine which is the actual photoelectron reference plane to consider in equations (1) and (2).

For such a study we can use nanostructured systems with structural tunability, which can be obtained by adsorbate-induced periodic faceting of vicinal surfaces. In the presence of adsorbates, periodic phase separation of adsorbate-covered and adsorbate-free facets may arise, since particular crystal orientations offer better substrate/adsorbate lattice matching [11–13]. An advantage of adsorbate-induced faceting is that by varying the coverage we readily tune the hill-and-valley structure. On stepped noble metal surfaces, such periodic nanostriped structures are particularly attractive for ARPES, since they exhibit Shockley-type surface states. The latter scatter strongly in nanoscale-sized features, such as steps or facet boundaries [18, 19]. In faceted, hill-and-valley systems they actually become confined within individual stripes, leading to two different states, each related to one of the alternating phases [20].

In this study, our tunable, striped system is created by deposition of submonolayer amounts of Ag on a vicinal Cu(111) surface [12, 21, 22]. The resulting system is characterized by alternating self-assembled nanostripes of Ag and Cu, both aligned along the step directions of the substrate (see figure 1), but with different crystal orientations. In fact, submonolayer deposition leads to Ag-covered step bunches, such that clean Cu facets are progressively depleted of steps, until Ag-free Cu areas become (111)-oriented stripes [12, 21]. Consequently, the Ag coverage has a direct influence on both the Ag and Cu stripe widths and on the local angle of the clean Cu facet (see figure 1). Confinement effects of Shockley states in these surfaces have already been reported [20, 23–25], exhibiting changes in the binding energy for both Ag and Cu surface states as a function of the stripe width and faceting periodicity, as well as changes in the photoelectron emission angle from the Cu stripes. In this work, we go a step beyond and introduce a Fourier analysis method of the ARPES data acquired for different photon energies (using synchrotron radiation) and periodicities (varying Ag coverage) so as to obtain the relevant reference direction of the surface electrons ejected from these uneven surfaces.

2. Experimental details

The Cu(223) substrate was atomically cleaned by standard cycles of Ar^+ sputtering and annealing to 700 K. The nanostriped Ag/Cu(223) system was prepared by deposition of Ag at room temperature (RT) in quantities smaller than one monolayer (ML), followed by a mild annealing at 450 K. This deposition treatment induces self-assembled heterogeneous double phases at the surface. The characteristic low-energy electron diffraction (LEED) pattern with sharp split spots of Cu stripes allows us to determine the Ag coverage ($\pm$0.05 ML) and the average terrace width d within Cu nanostripes [21, 22]. Previous STM and LEED studies show that annealing up to 700 K does not significantly influence the final stripe formation. This suggests that thermal equilibrium is reached and Cu–Ag alloying is not relevant [12, 21, 26].

The photoemission experiments were carried out in two synchrotron facilities. The first end station was located at the beamline F2.2 at HASYLAB (Hamburg, Germany) and covered the lower photon energy range 9–27 eV using a Seya-Namioka 1 m normal-incidence

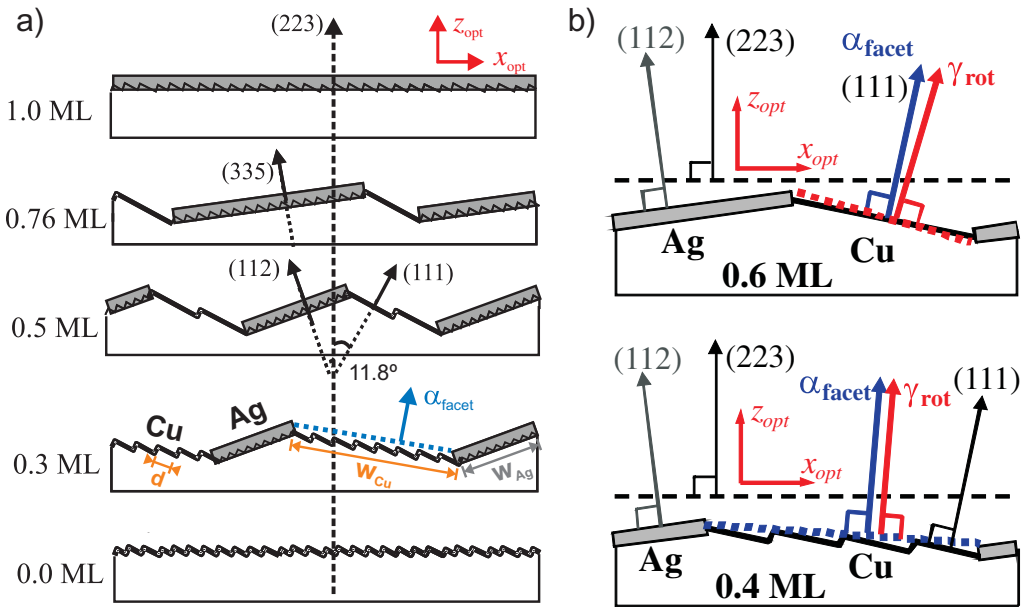

Figure 1. (a) Graphical representation of the evolution of the Ag/Cu(223) system with increasing Ag coverage (adapted from [22]). The amount of Ag is indicated on the left. Ag stripes (gray overlayers on the Cu substrate) grow in width (w_{Ag}), creating a step bunching effect underneath them. This consequently depletes the steps from the neighboring Cu facets and increases their average terrace size d so that facet angles are locally changed. The optical sample coordinate system is indicated at the top of the figure, i.e. x_{opt} is perpendicular to the steps and z_{opt} follows the surface normal direction. (b) Sketch of the correction angle (γ_{rot}) for 0.4 and 0.6 ML obtained from Fourier plots of figure 4. For 0.6 ML, γ_{rot} does not match α_{facet}, indicating that the (223) direction is not the appropriate ARPES reference plane for Cu facets (see text).

monochromator. The chamber was equipped with LEED, a quartz crystal microbalance and an in-vacuum mobile hemispherical analyzer (the energy/angular resolution was ~120 meV/ $\pm 1^{\circ}$). The second end station was located at the SU8 undulator beamline of the SuperAco storage ring at LURE (Orsay, France). Its plane grating monochromator was used to acquire the high-photon-energy data in the range from 22 to 110 eV. The vacuum chamber was also equipped with a LEED and a mobile electron hemispherical analyzer (the energy/angular resolution was ~80 meV/ $\pm 0.5^{\circ}$ at 21 eV photon energy). In both cases the data were acquired using horizontal polarized light in a p-polarized configuration, i.e. the incident photons had an angle of 70° with the sample optical normal. In this configuration the intensity of the surface states is maximized due to their p_z orbital character.

3. The Ag/Cu(223)-faceted system: structural evolution with Ag coverage

The Ag coverage-dependent morphology of the Ag/Cu stripe is graphically sketched in figure 1. The copper crystal is terminated by a (223) surface, vicinal to Cu(111) and with a miscut angle of 11.8° toward the $[\bar{1}\bar{1}2]$ high-symmetry direction. This surface presents flat terraces of {111}

orientation with an average width of 10.2 Å terminated with {100} steps of monoatomic height. When submonolayer amounts of Ag are deposited onto this substrate, Ag atoms aggregate into stripes aligned parallel to the substrate steps. Simultaneously, Cu stripes are formed that show variations on their local orientation. The lateral periodicity of the system is observed to greatly vary (between 100 and 300 Å) with Ag coverage [21].

Experimentally, the Ag/Cu(223) system shows three characteristic faceting regimes upon completion of the first Ag monolayer [12, 21, 22]. The first regime, named R_A hereafter, exists below ∼0.52 ML and shows a very regular stripe arrangement. The Ag facets grow with a fixed (112) orientation, independent of the coverage, which is 19.5° away from the (111) direction. In contrast, Cu stripes keep their vicinal-like morphology but change local facet orientation in order to maintain the macroscopic (223) orientation of the crystal. This is achieved by reducing the step density as the Ag coverage increases, i.e. a depletion of steps from the Cu facets is observed, which accumulate in Ag-covered (112) facets [12, 21]. Ideally, this process saturates at 0.61 ML (see equation (1) of [23]), when Cu facets become (111)-oriented planes after removing all their steps. However, due to surface defects the effective saturation takes place earlier, at the coverage of ∼0.52 ML.

The second regime, R_B, takes place between coverages of ∼0.52 and ∼0.76 ML. Here, the Ag facet orientation undergoes smooth transitions from the (112) to the (335) direction. New (335) facets originate from coalescence of the existing (112) facets, such that (335) bunches appear at the center of the new Ag facet, while the edges still keep the initial (112) orientation. Clean Cu facets with the (111) orientation remain, although they are quite narrow and irregular in size.

In the last regime, R_C, competition between (335) and (223) Ag facets is observed between ∼0.76 and 1 ML. The existing surface Cu areas are quite irregular and very small since at 1 ML coverage the Ag layer practically wets the whole surface.

4. Results

4.1. Electronic structure of Ag/Cu(223) nanostructures

The described structural properties of this system should correlate with its surface electronic structure. Such effects have already been reported for the present Cu(223) substrate and other Cu vicinals [19, 20, 23, 25]. But before describing our system electronically, it is convenient to briefly review the effects of regular step arrays on the Cu(111) Shockley state. The problem of the scattering of surface states at step arrays on noble metal surfaces has recently been revisited using cylindrical crystals [27]. The most characteristic observation is the size effect, namely the surface state shift toward the Fermi energy as the terrace width decreases, which reflects the repulsive character of the scattering potential of the steps [18, 27, 28]. On the other hand, in step arrays one can also observe Umklapp states of the superlattice, i.e. $\pm 2\pi/d$ surface state replica in the reciprocal space direction perpendicular to the steps ($k_{x,\mathrm{opt}}$ in figure 1) [18, 19, 28, 29]. Finally, a more subtle effect is the so-called switch of the modulation plane of the electron wave function, i.e. the 2D plane on which the surface state is defined and perpendicular to which the Fourier spectrum appears broadened. In fact, a transition is observed around ∼7° miscut from the (111) terrace plane to the average surface plane modulation [17, 30]. The former occurs when a large separation exists between steps and the latter occurs when this separation is notably reduced ($d < 17$ Å).

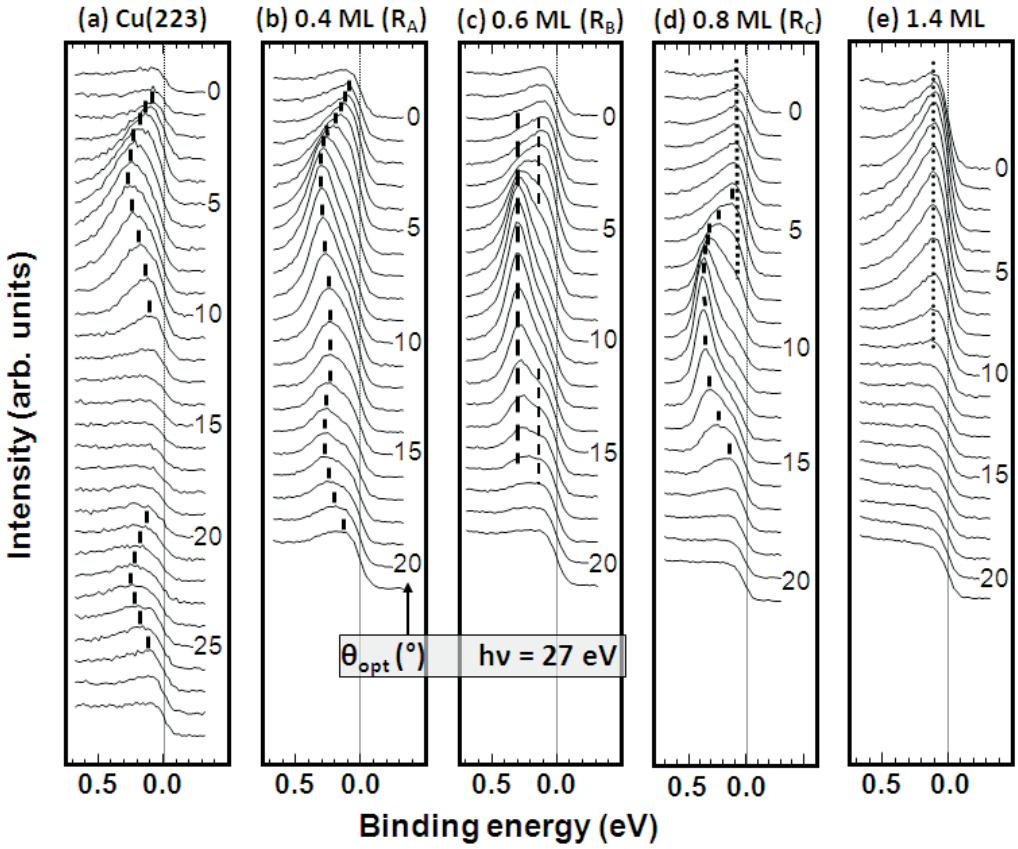

Figure 2. ARPES EDCs for selected Ag coverages deposited on Cu(223) acquired at RT using 27 eV photon energy: (a) clean surface, (b) 0.4 ML (R_A), (c) 0.6 ML (R_B), (d) 0.8 ML (R_C) and (e) 1.4 ML. The emission angle (indicated on the side) is steadily changed in the direction perpendicular to the steps and is referred to as the optical direction, i.e. the (223) direction. The ticks mark the Cu surface state position, whereas the dotted lines indicate the position of Ag states. A lack of resolution hinders the observation of the Ag state dispersion, as explained in the text.

Many of the aforementioned electronic features observed in infinite vicinal crystals are also found in the R_A regime of the Ag/Cu(223) striped system, as shown in [20]. In the present work, we complete the analysis with the observations made in the R_B and R_C coverage regimes. Figure 2 shows ARPES energy distribution curves (EDCs) acquired at 27 eV photon energy and RT for selected coverages. The emission angle scale refers to the average surface normal. Note that all features close to ∼0.4 eV binding energy are Cu-surface-state-like and correspond to the bare Cu stripe, whereas the intensity found closest to the Fermi energy for coverages above 0.6 ML is Ag-like and hence attributed to the Ag-covered facet [20]. The non-dispersiveness of the Ag states must not be mistaken for an intrinsic property related to the Ag facets. It is most likely a combination of our limited experimental resolution, high acquisition temperature (RT) and proximity to the Fermi energy, which cuts off the Ag peak and masks its dispersion (figures 2(d) and (e)).

From figures 2(a)–(d) the surface state dispersion corresponding to the stepped Cu stripes shows strong qualitative variations as a function of coverage. R_A is the region where the

strongest changes are observed since the average Cu terrace size d increases from 10.2 Å at 0 ML to ∼45 Å at ∼0.52 ML [22]. From R_A to R_B the dispersing 2D-like surface state (figure 2(a)) changes into a quasi-1D confined quantum well state (QWS, figure 2(c)), passing through the intermediate case of a 2D step superlattice state, with an apparent large gap opening at the superlattice zone edge (figure 2(b)).

The Cu state at the R_C regime unexpectedly recovers the band dispersion nature (figure 2(d)). Moreover, the binding energy of the bottom of the Cu state is the largest of all the presented data shown in figure 2, with a value of 0.37 eV. This value is similar to the Cu(111) surface state energy (0.39 eV) and clearly contrasts with the large upwards shifts observed for the clean Cu(223) (0.27 eV), 0.4 ML (0.30 eV) or 0.6 ML (0.32 eV) cases. The parabolic band dispersion is in disagreement, in essence, with the fact that Cu stripes in the R_C regime are extremely narrow, so that quantum well confinement would be expected. A similar observation has already been reported in [25] and explained as due to the effective quenching of the dipole barrier at Ag-decorated stripe edges, which makes the stripe boundaries transparent to surface electrons.

4.2. Electronic structure versus photon energy for Ag/Cu(223)

To determine the emission reference for the photoelectrons ejected from the nanostructured system depicted in figure 1, we investigate the surface states of the facets as a function of the photon energy. In this way, we can later perform a 3D analysis of the surface state wave vector, following equations (1) and (2) [20]. Figure 3 shows in grayscale several EDC carpets where the photoemission intensity is normalized to the incident photon flux and represented as a function of the electron binding energy and the emission angle (referred to as the optical normal). For optimal visualization, the Fermi step has been deconvoluted and removed from the spectra, and the grayplot's intensity scale range (dark being higher intensity) is common to all. Four different photon energies (22, 27, 50 and 70 eV) are shown for the selected coverages of figure 2. The bold lines indicate the angular position of the bottom of the Ag and Cu surface states, similar to figure 3 of [20] but comprising a larger dataset.

The EDC carpets of the clean substrate (figure 3(a)) and 0.40 ML (figure 3(b)) show the Cu surface state Umklapp for most of the photon energies investigated. Furthermore, the spectral intensity is transferred from the left (main) to the right (Umklapp) parabola as the incident photon energy is increased, in agreement with previous work [18–20, 31]. This is similar to LEED, where the intensity is maximum for in-phase interference and splits later when approaching out-of-phase conditions [32]. The main difference between the clean and the 0.40 ML images is the decrease in angular separation between Umklapps when Ag is present on the surface. This is direct evidence of an increase in the local terrace size in Cu stripes, associated with the fact that steps are being 'sucked' by densely stepped Ag-covered (112) facets that grow in size. As a consequence, the Cu facet at 0.40 ML has a local crystal orientation closer to (111) than the starting clean (223) surface.

Increasing the Ag coverage above the R_A phase saturation, i.e. when only single (111) terraces of Cu are visible in the Cu facets, alters the EDC carpets, as seen for 0.60 ML (figure 3(c)) and 0.80 ML (figure 3(d)). Firstly, there is no Umklapping of the Cu state, i.e. the two bands collapse into a single one, which still shows intensity modulation with photon energy. Secondly, we observe that the emission angle of the Cu stripe band does not significantly vary with photon energy and gets closer to the [111] crystal direction. Finally, as discussed

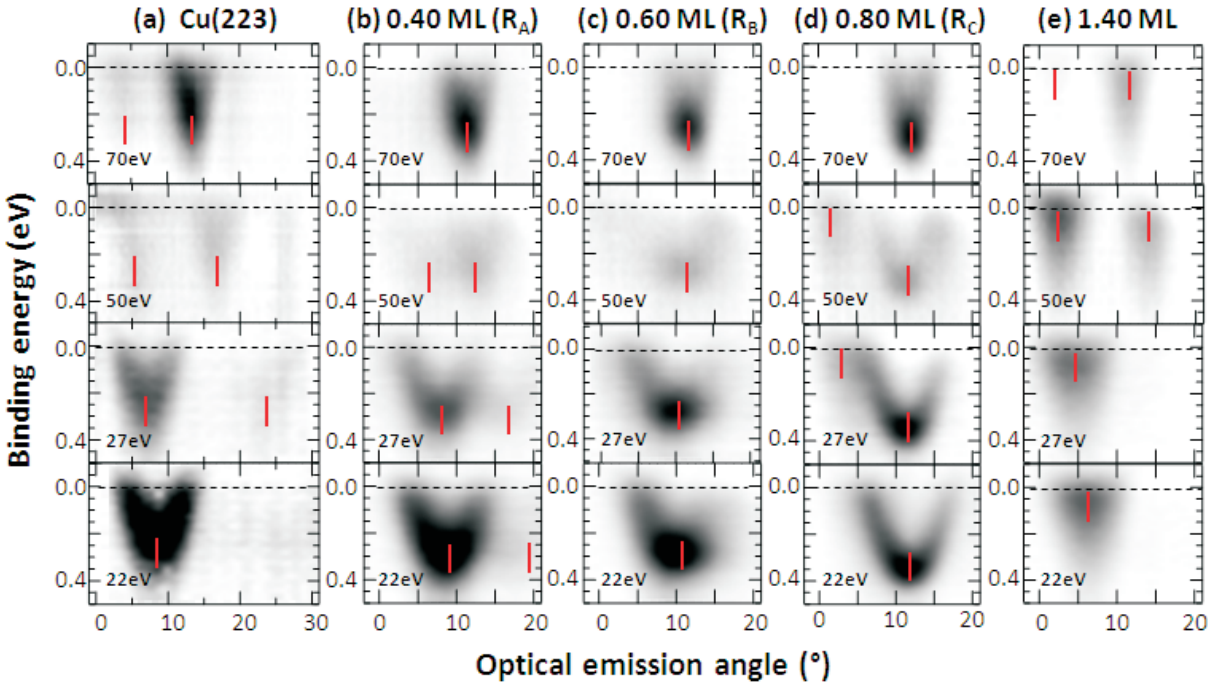

Figure 3. EDC carpets of the normalized photoemission intensity in grayscale (dark being more intense) as a function of the emission angle (referred to the optical normal) and photon energy for the selected Ag coverages of figure 2. For best visualization, the Fermi step has been removed from the data and the photoemission intensity scaled to a common range. The bold vertical lines mark the center of the surface state bands for Cu and Ag.

previously, the surprising change from QWS at 0.6 ML to the dispersive band at 0.80 ML is neatly observed.

Above 1 ML, as is the case for figure 3(e), we no longer observe Cu states. The peaks are related to Ag states and show behavior similar to the clean case, i.e. both Umklapping and intensity modulation are observed as a function of photon energy. This state is already present at 0.80 ML (figure 3(d)) for 27 and 50 eV. As mentioned previously, the low instrumental resolution hinders us from observing any dispersion due to its proximity to the Fermi energy. Therefore, we shall focus our discussion on the emission reference of the photoemitted electrons on the Cu state alone.

5. Discussion: determination of the reference plane for photoemitted electrons in Ag/Cu(223)

5.1. Average surface plane analysis

We observe notable differences in the angular position of the Cu bands, depending on both Ag coverage and photon energy in figure 3. To understand them we elaborate the so-called 3D wave vector plots in figure 4. These display parallel and perpendicular momentum values ((k_x, k_z) points) for the surface band minimum (band bottom), as calculated directly from

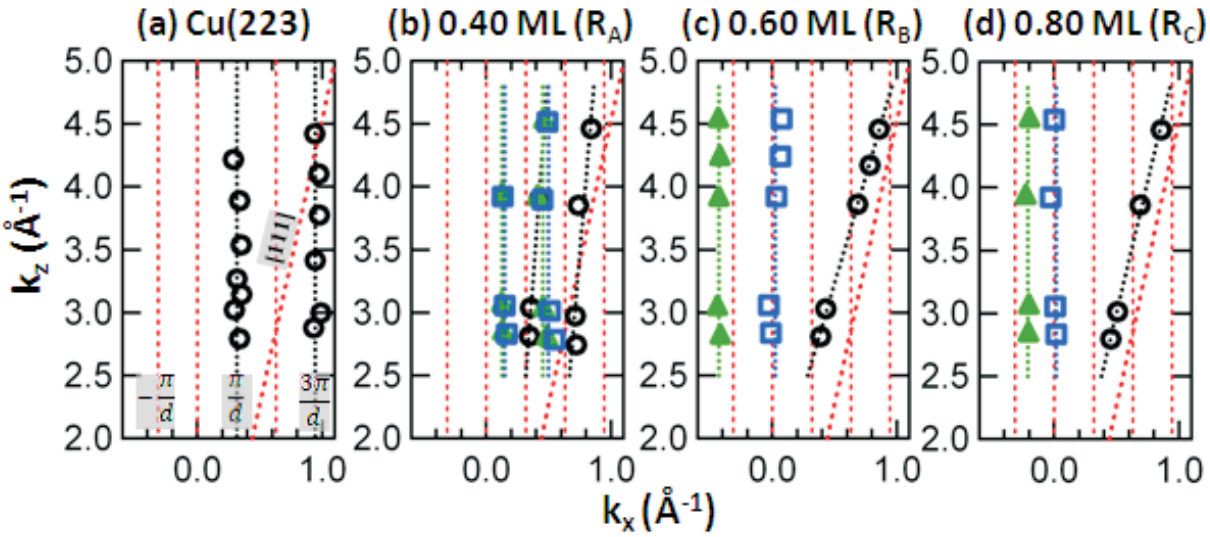

Figure 4. Wave vector plots of the Cu state for the previously selected Ag coverages. The black circles indicate $(k_{x,\mathrm{opt}}, k_{z,\mathrm{opt}})$ pairs for the bottom of the Cu surface state when θ is referred to the optical (average) surface in equations (1) and (2). The green triangles correspond to new $(k_{x,\mathrm{rot}}, k_{z,\mathrm{rot}})$ pairs after applying a *direct rotation* of the wave vector reference system to $(k_{x,\mathrm{opt}}, k_{z,\mathrm{opt}})$ data. The blue squares mark $(k_{x,\mathrm{facet}}, k_{z,\mathrm{facet}})$ pairs referred to the local facet after using a *structural correction* that considers the local facet plane as the reference direction θ in equations (1) and (2). Linear fits to each point type are shown as dotted lines of equal colors. The vertical discontinuous lines common to all panels indicate multiples of $k_x = \pi/d$ of the substrate, whereas the tilted discontinuous line marks the [111] direction, as shown in the left panel.

equations (1) and (2)[8]. In reality, wave vector plots describe the 3D Fourier composition of the surface state [20, 30]. As discussed for vicinal surfaces, in wave vector plots data points line up along 'diffraction' rods perpendicular to the modulation plane of the wave function. This is the plane in which the 2D surface state is defined, which in practice means the plane where the parallel momentum component remains constant with varying photon energy, as expected for any 2D state. Each of the panels in figure 4 shows k_z versus k_x sets using different reference directions and data analysis frameworks, which will be explained in the following. The data and linear fits correspond only to the Cu-like state below 1 ML, shown in figures 2 and 3.

We begin with a well-documented case, i.e. the clean substrate, which is shown in figure 4(a) [20, 31]. There are only two relevant directions: the optical (average surface) and the (111) (terraces). Such a vicinal surface with narrow terraces has the average surface plane as the modulation plane of the surface state [20, 31]. Therefore, when plotting the $(k_{x,\mathrm{opt}}, k_{z,\mathrm{opt}})$ pairs calculated with respect to the (223) direction (black open circles), we observe that they fall along two parallel vertical lines with constant k_x values at $\pi/d = 0.31\,\text{Å}^{-1}$ and $3\pi/d = 0.94\,\text{Å}^{-1}$. These correspond to the first and second Brillouin zone (BZ) edges of the step superlattice, as expected for Shockley-like states in surfaces away from the (111) direction. Thus, we

[8] We use as the crystal internal potential $V_0 = 13.5$ after [16] and [17].

straightforwardly conclude that for the clean substrate, equations (1) and (2) hold with the expected photoelectron reference direction, i.e. the average surface (223) direction, θ being the emission angle with respect to its normal.

For Cu nanostripes evolving from the Ag/Cu(223) system, the data exhibit more complex behavior. In the case of 0.4 ML of Ag (figure 4(b)) Umklapps in the EDC carpets give rise to two sets of data points. Assuming equations (1) and (2) and the optical surface as the reference direction of the photoelectron (as previously done for the Cu(223) surface), the two sets of points are aligned along two split lines, but tilted by 4.5° with respect to the average surface normal. This angle agrees, within the experimental error, with the local Cu facet angle reported by STM for this coverage, which is 4.8° from the (223). In the case of 0.6 ML (figure 4(c)) the alignment of the $(k_{x,\mathrm{opt}}, k_{z,\mathrm{opt}})$ points calculated with respect to the optical normal further rotates to 16°.[9] This is even larger than the local Cu facet angle, which in this case is the (111) terrace (11.8° with respect to the optical normal). Similar behavior is found for 0.80 ML (figure 4(d)), where we observe that the $(k_{x,\mathrm{opt}}, k_{z,\mathrm{opt}})$ values are aligned with a tilt of 13°. This is closer, although still larger, than the flat (111) terrace orientation where we expect our electron wave function modulation.

Assuming the principle that the parallel momentum is a good quantum number for surface states ($k_x = \mathrm{const}$ in wave vector plots), the presence of tilted rods in wave vector plots may simply be interpreted in terms of a (somewhat arbitrary) surface state modulation plane, which would be defined by such rods at 4.5°, 16° and 13° with respect to the average surface normal for 0.4, 0.6 and 0.8 ML facets, respectively. Therefore, a constant parallel momentum ($k_x = \mathrm{const}$) is simply obtained after changing to the reference system of the wave vector (modulation plane), i.e. by rotating all $(k_{x,\mathrm{opt}}, k_{z,\mathrm{opt}})$ pairs by the respective tilt angles. We name this process the *direct rotation* correction of the wave vector reference system. The relation to momentum with the optical reference system can be readily determined:

$$k_{x,\mathrm{rot}} = \left(k_{x,\mathrm{opt}} - \frac{k_{z,\mathrm{opt}}}{m}\right)\cos(\gamma_{\mathrm{rot}}), \tag{3}$$

$$k_{z,\mathrm{rot}} = \frac{k_{z,\mathrm{opt}}}{\cos(\gamma_{\mathrm{rot}})} + \tan(\gamma_{\mathrm{rot}}) \cdot (-A) \cdot \cos(90^\circ - \gamma_{\mathrm{rot}}), \tag{4}$$

where m and A are, respectively, the slope and the intercept of the linear regressions shown in figure 4 and γ_{rot} is the rotation angle defined between $k_{z,\mathrm{opt}}$ and the line fit. The green triangles in figures 4(b)–(d) show the resulting $(k_{x,\mathrm{rot}}, k_{z,\mathrm{rot}})$ pairs after the application of such a transformation to the initial $(k_{x,\mathrm{opt}}, k_{z,\mathrm{opt}})$ values. For the 0.40 ML case (figure 4(b)) the rotation by $\gamma_{\mathrm{rot}} = 4.5^\circ$ obtained from the fit gives two vertical lines separated by $\Delta k_{x,\mathrm{rot}} = 0.35\ \text{Å}^{-1}$, where the first line is located at precisely $k_{x,\mathrm{rot1}} = \frac{1}{2}\Delta k_{x,\mathrm{rot}}$. Similar to the case of the clean substrate [31], the vertical lines correspond to the 1st and 2nd BZ edges of the Cu facet step superlattice. Such momentum relations correspond to facets with a terrace size of $d = 18$ Å and a facet angle of 6.6° with respect to the (111) direction, values that are basically identical to those obtained from STM images ($d = 17$ Å and 7°) [12, 22]. In this way, there is agreement between the local facet angle α_{facet} and the rotation angle γ_{rot}, as sketched at the bottom of figure 1(b).

[9] The tilt angle obtained for the QWS case at 0.6 ML of Ag is likely to be subject to errors when determining its bottom angular position given its nondispersive character.

The *direct rotation* of the wave vector reference system, however, fails when addressing Ag coverages above 0.5 ML. In such cases the $k_{x,\mathrm{rot}}$ values obtained through equations (3) and (4) are negative and hence senseless. Therefore, the modulation of the surface state in the plane defined by γ_{rot} cannot appropriately explain wave vector plots, suggesting that one must consider a different reference plane of the photoemitted electron, i.e. the crystal plane that defines $k_{||}$ and $k_{\perp}$ in equations (1) and (2). The γ_{rot} turns out to be an arbitrary angle for coverages above 0.5 ML since it is not matching any structural plane, as represented at the top of figure 1(b).

5.2. Local nanofacet plane analysis

It is now evident that equations (1) and (2) should be referred to the changing nanoscopic surface plane in Cu nanostripes of the Ag/Cu(223) system, i.e. the Cu local facet angle appears as the reference system for photoelectrons:

$$\theta = \theta_{\mathrm{opt}} - \alpha_{\mathrm{facet}}. \tag{5}$$

In the present Ag/Cu(223) system, the Cu nanostripe angle is well known from STM and LEED analyses. In the R_A regime up to 0.61 ML the local facet angle α_{facet} can be analytically derived as [23]

$$\alpha_{\mathrm{facet}} = \alpha_0 - \arcsin\left(\frac{\sin\alpha_0 - \Theta\cdot\sin\alpha_{\mathrm{Ag}}}{1-\Theta}\right), \tag{6}$$

where $\alpha_0 = 11.8^\circ$ is the angle between the (111) and the (223) optical directions, $\alpha_{\mathrm{Ag}} = 19.5^\circ$ is the angle between the (111) and the (112) Ag facets, and Θ is the total Ag coverage. Above 0.61 ML saturation, i.e. for the R_B and R_C regimes, the Cu stripes have a fixed (111) direction, which means a fixed $\alpha_{\mathrm{facet}} = 11.8^\circ$ in equation (5). Therefore, equations (1) and (2) can be rewritten for each nanostripe orientation assuming equations (5) and (6), and correspondingly correct wave vector plots in figure 4. We term this correction as the *structural correction* of the photoelectron reference plane. The graphs in figures 4(b)–(d) show as blue open squares the resulting $(k_{x,\mathrm{facet}}, k_{z,\mathrm{facet}})$ pairs of the Cu state after applying the *structural correction* to equations (1) and (2). For 0.40 ML $\alpha_{\mathrm{facet}} = 4.88^\circ$ so that correcting this angle in figure 3(b) results in $\Delta k_{x,\mathrm{facet}} = 0.35\,\text{Å}^{-1}$, i.e. equivalent to a terrace width of 8 Å (matching the value of 4.8° obtained from LEED and STM). For the higher coverages of 0.60 and 0.80 ML the angle that the spectra must be corrected is 10.91° and 11.8°, respectively. In this way, we obtain $k_{x,\mathrm{facet}} \simeq 0\,\text{Å}^{-1}$, i.e. coincident with the (111) direction.

Note, however, that structural details will be basically unknown in most systems, and hence the *structural correction* of equations (5) and (6) cannot be generally performed. What should thus be the way of determining the reference orientation for ARPES data in a general case? We may simply come back to the premise that the wave vector scale must be meaningful, i.e. that diffraction rods in wave vector plots like those in figure 4 should be vertical, but applying this premise to (k_x, k_z) data determined from equations (1) and (2). In other words, we can empirically search the angle δ at which the resulting k_x surface wave vector has a constant value. Thus, we make $\theta = \theta_{\mathrm{opt}} - \delta$ in equations (1) and (2) and find the reference plane orientation for each Ag coverage. In this way, k_x will always be constant upon photon energy changes (experimental points will be vertically aligned in figure 4) and the data will be placed at exactly $((2n+1)/2)\times\pi/d$ diffraction rods in figure 4. The angle δ is therefore a correction to the previous optical angle and so it gives the reference direction for the emitted electrons. Note, however, that no link to the existing surface morphology is

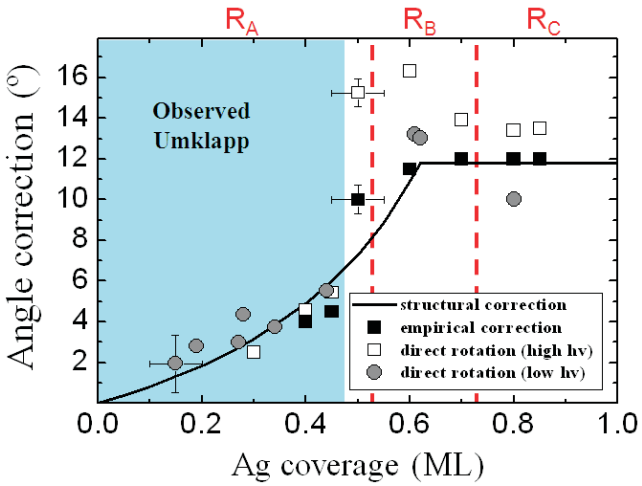

Figure 5. Comparison of the *structural correction* (solid line) to equations (1) and (2), as calculated from equation (6), and the photoemission submitted to a *empirical correction* of the photoelectron reference plane ($\theta = \theta_{\text{opt}} - \delta$ in equations (1) and (2)) that forces data points to line up in vertical rods in the diffraction plots. Graph details: the gray circles and open squares correspond to the *direct rotation* method when applied respectively to the low or to the high photon energy data. Note that the *empirical correction* method (filled black squares) can only be applied to data acquired at higher energy. These have a smaller overall error than the lower photon energy data (the error of each method is indicated for one of its markers). The shaded area shows the coverage range where Umklapps can be observed for the higher photon energy data. The three structural regimes are indicated by vertical dotted lines.

done and hence only an *empirical correction* to the photoelectron reference plane is done. In figure 5 we compare ARPES data modified through such *empirical correction*, with the *structural correction* (solid line) derived from equations (5) and (6), and hence based on STM and LEED data. Data points from the *empirical correction* follow closely the *structural correction* black line, confirming that the Cu surface state in the stepped nanostripe is referred to the local facet. What is particularly remarkable is the case of the dispersing band found for very narrow (111)-oriented nanostripes at 0.8 ML. In this case, the *direct rotation* of the wave vector reference system does not work, but the *empirical correction* is coincident with the *structural correction*. This means that for very narrow Cu stripes delimited by Ag-decorated steps, 2D electrons propagate in the (111) plane, without backscattering at stripe edges. This behavior was previously deduced from non-faceted, Ag/Cu nanostripe systems [25].

In figure 5, a slight deviation might be present around ∼0.5 ML. At this coverage the system is close to saturation, and hence stripes are defined by very few (2–3) large (> 20 Å) terraces [23], with significant terrace size variations. Interestingly, this is also the terrace size at which a switch in the electronic wavefunction modulation plane from average (nanostripe) to (111) terrace has been claimed [17, 30]. In fact, data in vicinal surfaces of [17, 30] were also analyzed using the average surface plane as the reference direction of the photoelectron,

resulting in 'diffraction rods' that lined up along the [111] crystal direction, similar to that in figures 4(c) and (d). This coincidence with the nanostripe system strongly suggests that both the photoelectron reference and the modulation plane must actually be the same, and that lateral disorder, and hence surface state coherence, is the key determining property. For coherent arrays of steps, this photoelectron-reference/modulation plane is the average surface, whereas incoherent terraces, which decouple surface states, emit photoelectrons non-coherently, modulated on the terrace plane.

6. Conclusions

In summary, we have studied by ARPES the effect that nanostructured surfaces have on the photoemitted electrons when the local orientation of the surface at the nanoscale does not correspond to the optical, macroscopic plane. We chose the Ag/Cu(223) system because it shows an alternating and regular set of Ag and Cu nanostripes that can be tuned with Ag coverage and where surface electrons can be confined. By introducing different analysis methods to investigate the 3D Fourier components, we unambiguously demonstrate that electrons photoemitted from the Cu facets are not referred to the overall optical surface but to its local facet direction. If the geometry is unknown, the reference plane can be defined from the complete Fourier analysis of the (nano-object confined) electron states through diffraction plots.

The implications of such a fundamental result are far reaching, since we expect any periodic local nanoscopic structure to define its own emission reference plane. Our observation has the prospect to be even more important when nano-focused ARPES becomes routinely available to the scientific community at synchrotron facilities. This technique avoids spatial averaging over mesosocopic arrays, offering the possibility to study new types of nanostructures.

Acknowledgments

We acknowledge A R Bachmann, F Ostendorf, J Kuntze and S Speller for their support and collaboration during these experiments. We also acknowledge the help and support provided by the staff of HASYLAB and LURE during data acquisition. JLC and AM acknowledge the Spanish Ministerio de Ciencia e Innovación (MICINN) for financial support through the research program Ramón y Cajal. JEO acknowledges support from the Spanish MICINN (MAT2010-21156-C03-01), the Basque Government (IT-257-07) and the DIPC (sabbatical program). EGM acknowledges support from the Spanish MICINN (FIS2008-00399).

References

[1] Jeong H-C and Williams E D 1999 *Surf. Sci. Rep.* **34** 171
[2] Rosei F 2004 *J. Phys.: Condens. Matter* **16** S1373
[3] Xu M, Okada A, Yoshida S and Shigekawa H 2009 *Appl. Phys. Lett.* **94** 073109
[4] Berbezier I and Ronda A 2009 *Surf. Sci. Rep.* **64** 47
[5] Bertel E and Lehmann J 1998 *Phys. Rev. Lett.* **80** 1497
[6] Berge K, Gerlach A, Meister G, Goldmann A and Bertel E 2004 *Phys. Rev.* B **70** 155303
[7] Malterre D, Kierren B, Fagot-Revurat Y, Pons S, Tejeda A, Didiot C, Cercellier H and Bendounan A 2007 *New J. Phys.* **9** 391

[8] Gambardella P, Dallmeyer A, Maiti K, Malagoli M C, Eberhardt W, Kern K and Carbone C 2002 *Nature* **416** 301
[9] Zaki N, Potapenko D, Johnson P D and Osgood R M 2009 *Phys. Rev.* B **80** 155419
[10] Rousset S, Repain V, Baudot G, Garreau Y and Lecoeur J 2003 *J. Phys.: Condens. Matter* **15** S3363
[11] Fölsch S, Helms A, Riemann A, Repp J, Meyer G and Rieder K H 2002 *Surf. Sci.* **497** 113
[12] Bachmann A R, Speller S, Mugarza A and Ortega J E 2003 *Surf. Sci.* **526** L143
[13] Bruns D, Gevers S and Wollschläger J 2011 *Surf. Sci.* **605** 861
[14] Hüfner S 2003 *Photoelectron Spectroscopy: Principles and Applications* 3rd edn (Berlin: Springer)
[15] Plummer E W and Eberhardt W 1982 *Adv. Chem. Phys.* **49** 533
[16] Matzdorf R 1998 *Surf. Sci. Rep.* **30** 153
[17] Ortega J E, Mugarza A, Närmann A, Rubio A, Speller S, Bachmann A R, Lobo J, Michel E G and Himpsel F J 2001 *Surf. Sci.* **482–485** 764
[18] Mugarza A and Ortega J E 2003 *J. Phys.: Condens. Matter* **15** S3281
[19] Zaki N, Knox K, Johnson P D, Fujii J, Vobornik I, Panaccione G and Osgood R M 2011 *Phys. Rev.* B **83** 205420
[20] Lobo J, Michel E G, Bachmann A R, Speller S, Kuntze J and Ortega J E 2004 *Phys. Rev. Lett.* **93** 137602
[21] Bachmann A R, Mugarza A, Ortega J E and Speller S 2001 *Phys. Rev.* B **64** 153409
[22] Bachmann A R, Ostendorf F and Speller S 2003 *J. Phys.: Condens. Matter* **15** S3337
[23] Ortega J E, Ruíz-Osés M and Kuntze J 2005 *Phys. Rev.* B **72** 195416
[24] Mugarza A, Schiller F, Kuntze J, Cordón J, Ruiz-Oses M and Ortega J E 2006 *J. Phys.: Condens. Matter* **18** S27
[25] Schiller F, Ruíz-Osés M, Cordón J and Ortega J E 2005 *Phys. Rev. Lett.* **95** 066805
[26] Sprunger P T, Laegsgaard E and Besenbacher F 1996 *Phys. Rev.* B **54** 8163
[27] Ortega J E, Corso M, Abd-el-Fattah Z M, Goiri E A and Schiller F 2011 *Phys. Rev.* B **83** 085411
[28] Baumberger F, Hengsberger M, Muntwiler M, Shi M, Krempasky J, Patthey L, Osterwalder J and Greber T 2004 *Phys. Rev. Lett.* **92** 196805
[29] Mugarza A, Mascaraque A, Repain V, Rousset S, Altmann K N, Himpsel F J, Koroteev Yu M, Chulkov E V, García de Abajo F J and Ortega J E 2002 *Phys. Rev.* B **66** 245419
[30] Ortega J E, Speller S, Bachmann A R, Mascaraque A, Michel E G, Närmann A, Mugarza A, Rubio A and Himpsel F J 2000 *Phys. Rev. Lett.* **84** 6110
[31] Lobo J, Michel E G, Bachmann A R, Speller S, Roca L, Kuntze J and Ortega J E 2003 *J. Vac. Sci. Technol.* A **21** 1194
[32] Henzler M 1976 *Appl. Phys.* A **9** 11–7